Configurational Isomerism in Bis(*N*-alkylsalicylaldiminato)nickel(II) Complexes: The Equilibrium Planar ⇌ Tetrahedral and Its Effect on the Kinetics and Mechanism of Ligand Substitution

Rainer Knoch, Horst Elias,* and Helmut Paulus[†]

Anorganische Chemie III, Institut für Anorganische Chemie, Technische Hochschule Darmstadt, Petersenstrasse 18, D-64287 Darmstadt, Federal Republic of Germany

Received December 21, 1994[⊗]

A series of bis(*N*-alkylsalicylaldiminato)nickel(II) complexes Ni(XYsal-R) = NiA_2 with different combinations of substituents X (= *tert*-butyl, isopropyl, isobutyl, NO_2, Br), Y (= methyl, H), and alkyl groups R (= H, methyl, ethyl, *n*-propyl, isopropyl, *n*-butyl, isobutyl, *tert*-butyl, neopentyl) were prepared and characterized by their vis/near-IR absorption spectra and magnetic moments (XYsal-R = anion of *N*-alkyl-3-X-5-Y-salicylaldimine). X-ray structure analysis of Ni(3-*tert*-butyl-5-methylsal-Et)$_2$ (= $C_{28}H_{40}N_2O_2Ni$; monoclinic, $P2_1/c$; a = 12.188(4), b = 11.455(4), and c = 18.852(6) Å, β = 97.66(1)°; Z = 4; R_w = 0.0367) and of the corresponding Zn(II) complex (= $C_{28}H_{40}N_2O_2Zn$; monoclinic, $C2/c$; a = 27.14(2), b = 13.17(1), and c = 18.30(2) Å, β = 120.64(2)°; Z = 8; R_w = 0.0357) confirms a distorted planar geometry of the NiN_2O_2 coordination core and tetrahedral coordination of the zinc. The equilibrium constants K_1 and K_2 for the formation of the various pyridine adducts NiA_2·py and NiA_2·2py, respectively, were determined by spectrophotometric titration in acetone. Variable-temperature ^{1}H NMR measurements led to the equilibrium constants $K_{p,t}$ for the fast configurational isomerization of complexes NiA_2 in organic solution according to NiA_2 (planar) ⇌ NiA_2 (tetrahedral). Conventional and stopped-flow spectrophotometries were used to study the kinetics of displacement of the two bidentate ligands in NiA_2 by tetradentate ligands H_2B = H_2salen (= *N,N'*-disalicylidene-1,2-diaminoethane), H_2salpren (= *N,N'*-disalicylidene-1,3-diaminopropane), and H_2sal(Me)$_2$en (= *N,N'*-disalicylidene-1,2-diamino-2-methylpropane) in acetone solution. Ligand displacement follows second-order kinetics, rate = $k_{H_2B}[NiA_2][H_2B]$. For complexes Ni(3-*tert*-butyl-5-methylsal-R)$_2$ and H_2B = H_2salen, rate constant k_{H_2B} spans from 3.75 × 10^4 M^{-1} s^{-1} for R = methyl to 4.4 × 10^{-3} M^{-1} s^{-1} for R = *tert*-butyl at 298 K. The activation entropy ranges from −52.5 J mol^{-1} K^{-1} for Ni(3-isobutylsal-ethyl)$_2$ to −138 J mol^{-1} K^{-1} for Ni(3-nitro-5-methylsal-isopropyl)$_2$. The parameters K_1, K_2, $K_{p,t}$, and k_{H_2B} are governed by the bulkiness and specific combination of the various substituents X and alkyl groups R. The size of these parameters allows meaningful conclusions concerning the associatively controlled mechanism of ligand displacement.

Introduction

The $3d^8$ metal center Ni(II) offers a rich coordination chemistry with a variety of coordination numbers and coordination geometries. An interesting stereochemical aspect is that, with several bidentate chelate ligands[1,2] such as *N,N'*-dialkyl-2-aminotroponeimines, for example, Ni^{2+} ions form four-coordinate complexes Ni(R$_2$-ati)$_2$,[3] which are subject to a fast configurational change in solution. The planar diamagnetic isomer is in equilibrium with the tetrahedral paramagnetic isomer, and increasing steric demands of R shift the equilibrium toward the tetrahedral configuration.[1,2,4]

We have studied the kinetics of ligand substitution according to eqs 1 and 2 in a variety of systems (M = Cu, Ni; HA = salicylaldimine; HB = β-diketone; H_2B = H_2salen[3]) by exploring solvent effects,[5] substituent effects,[6] the effect of steric hindrance and axial blocking,[7] stacking interactions,[8] chiral discrimination,[9] and intermediate formation.[10] It has been shown for reaction 3 that H_2salen attacks only the planar configurational isomer of Ni(R$_2$-ati)$_2$[3], the tetrahedral one being kinetically inert.[4]

$$MA_2 + 2\,HB \rightleftharpoons MB_2 + 2\,HA \quad (1)$$

$$MA_2 + H_2B \rightleftharpoons MB + 2HA \quad (2)$$

$$Ni(R_2\text{-ati})_2 + H_2\text{salen} \rightleftharpoons Ni(\text{salen}) + 2\,R_2\text{-atiH} \quad (3)$$

[†] Fachbereich Materialwissenschaft, Technische Hochschule Darmstadt.

[⊗] Abstract published in *Advance ACS Abstracts,* June 15, 1995.

(1) Schumann, M.; von Holtum, A.; Wannowius, K. J.; Elias, H. *Inorg. Chem.* **1982**, *21*, 606.

(2) (a) Holm, R. H.; Everett, G. W., Jr.; Chakravorty, A. *Prog. Inorg. Chem.* **1966**, *7*, 83. (b) Holm, R. H., O'Connor, M. *Ibid.* **1971**, *14*, 241.

(3) Abbreviations: Ni(R$_2$-ati)$_2$ = bis(*N,N'*-dialkyl-2-aminotroponeiminato)nickel(II); H_2salen = H_2B^1 = *N,N'*-disalicylidene-1,2-diaminoethane; Ni(XYsal-R)$_2$ = bis(*N*-alkyl-3-X-5-Y-salicylaldiminato)nickel(II), substituents X, Y, and R, respectively, H = hydrogen, Me = methyl, Et = ethyl, *n*-Pr = 1-propyl, *i*-Pr = isopropyl, *n*-Bu = 1-butyl, *i*-Bu = 2-methylpropyl, *t*-Bu = *tert*-butyl, *neo*-Pe = neopentyl; H_2salpren = H_2B^2 = *N,N'*-disalicylidene-1,3-diaminopropane; H_2sal(Me)$_2$en = H_2B^3 = *N,N'*-disalicylidene-1,2-diamino-2-methylpropane.

(4) Schumann, M.; Elias, H. *Inorg. Chem.* **1985**, *24*, 3187.

(5) (a) Elias, H.; Fröhn, U.; von Irmer, A.; Wannowius, K. J. *Inorg. Chem.* **1980**, *19*, 869. (b) Elias, H.; Reiffer, U.; Schumann, M.; Wannowius, K. J. *Inorg. Chim. Acta* **1981**, *53*, L65. (c) Elias, H.; Muth, H.; Niedernhöfer, B.; Wannowius, K. J. *J. Chem. Soc., Dalton Trans.* **1981**, *9*, 1825. (d) Elias, H.; Fröhn, U.; Giegerich, G.; Stenger, M.; Wannowius, K. J. *J. Chem. Soc., Dalton Trans.* **1982**, *3*, 577. (e) Elias, H.; Wannowius, K. J. *Inorg. Chim. Acta* **1982**, *64*, L157. (f) Elias, H.; Muth, H.; Sahm, H.; Volz, H.; Wannowius, K. J. *Inorg. Chim. Acta* **1983**, *68*, 163.

(6) Elias, H.; Hasserodt-Taliaferro, C.; Hellriegel, L.; Schönherr, W.; Wannowius, K. J. *Inorg. Chem.* **1985**, *24*, 3192.

(7) (a) Knoch, R.; Wilk, A.; Wannowius, K. J.; Reinen, D.; Elias, H. *Inorg. Chem.* **1990**, *29(19)*, 3799. (b) Segla, P.; Elias, H. *Inorg. Chim. Acta* **1988**, *149*, 259.

(8) Büsing, B.; Elias, H.; Eslick, I.; Wannowius, K. J. *Inorg. Chim. Acta* **1988**, *150*(2), 223.

(9) Warmuth, R.; Elias, H. *Inorg. Chem.* **1991**, *30*, 5027.

(10) Hoss, H.; Elias, H. *Inorg. Chem.* **1993**, *32*, 317.

0020-1669/95/1334-4032$09.00/0

Chart 1. Structural Formulas of the Complexes and Ligands and Abbreviations[3]

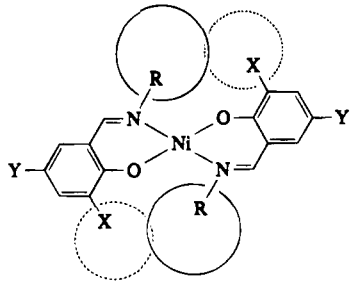

X	Y	R
*t*Bu	Me	H, Me, Et, *n*Pr, *i*Pr, *n*Bu, *i*Bu, *t*Bu, *neo*Pe
*i*Pr	H	Et, *i*Pr
*i*Bu	H	Et, *i*Pr
NO_2	Me	Et, *i*Pr
Br	Me	Et, *i*Pr

Ni(XYsal-R)$_2$

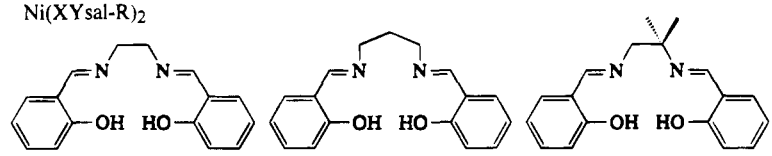

H_2salen = H_2B^1 H_2salpren = H_2B^2 H_2sal(Me)$_2$en = H_2B^3

The present contribution extends the study of configurational isomerism and its kinetic implications to substituted bis(*N*-alkylsalicylaldiminato)nickel(II) complexes (Ni(XYsal-R)$_2$), for some of which the equilibrium planar ⇌ tetrahedral was reported earlier.[2,11] For X = Y = H and R is small, complexes Ni(XYsal-R)$_2$ prefer the planar trans-N_2O_2 coordination geometry (see Chart 1) and tend to become octahedral in the presence of bases such as pyridine (see eq 4). It follows from model considerations that steric repulsion and, as a consequence,

$$\text{Ni(sal-R)}_2 + 2\text{py} \overset{K_1}{\rightleftharpoons} \text{Ni(sal-R)}_2\text{(py)} + \text{py} \overset{K_2}{\rightleftharpoons} \text{Ni(sal-R)}_2\text{(py)}_2 \quad (4)$$

tetrahedral distortion occur for large R groups interacting with the neighboring phenolic oxygen and/or large X substituents. It was therefore decided to use the combination of bulky X substituents and sterically more or less demanding R groups to prepare a series of complexes Ni(XYsal-R)$_2$ with a variable degree of tetrahedral distortion. The size of the constant $K_{p,t}$, which can be obtained from the temperature dependence of the paramagnetic shift of the ^{1}H NMR spectra of Ni(XYsal-R)$_2$, is a measure of the equilibration in solution according to eq 5.

$$\underset{\text{planar } (S=0)}{\text{Ni(XYsal-R)}_2} \overset{K_{p,t}}{\rightleftharpoons} \underset{\text{tetrahedral } (S=1)}{\text{Ni(XYsal-R)}_2} \quad (5)$$

The kinetic parameters describing ligand substitution in acetone solution according to eq 6 were determined for the tetradentate ligands H_2B = H_2B^1, H_2B^2, and H_2B^3 (see Chart 1) reacting with the complexes Ni(XYsal-R)$_2$ listed in Chart 1.

$$\text{Ni(XYsal-R)}_2 + \text{H}_2\text{B} \rightarrow \text{NiB} + 2\,\text{H-XYsal-R} \quad (6)$$

The rate data obtained are compared to the thermodynamic parameters $K_{p,t}$, K_1, and K_2 in order to correlate reactivity and state of coordination.

Experimental Section

$Ni(CH_3COO)_2{\cdot}4H_2O$, $NiBr_2$, $Zn(CH_3COO)_2{\cdot}2H_2O$, and the solvent acetone were reagent grade. The various amines and diamines used for the synthesis of the aldimines H-XYsal-R and salen-like ligands H_2B by condensation with the corresponding aldehydes

$$\text{H-XYsal} + \text{R-NH}_2 \rightarrow \text{H-XYsal-R} + \text{H}_2\text{O} \quad (7a)$$

$$2\text{H-XYsal} + \text{diamine} \rightarrow \text{H}_2\text{B} + 2\text{H}_2\text{O} \quad (7b)$$

H-XYsal according to eqs 7a and 7b, respectively, were commercially available. The substituted salicylaldehydes[3] H-*t*-BuMesal,[12] H-*i*-PrHsal,[13] H-*i*-BuHsal,[13] H-NO_2Mesal,[14,15] and H-BrMesal[16] were prepared according to published procedures. Except for H-*t*-BuMesal-H, H-*t*-BuMesal-Me, and H-*t*-BuMesal-Et, Schiff base formation according to eq 7a was carried out in ethanol with stoichiometric amounts of aldehyde and amine RNH_2 at 60 °C. After evaporation of the solvent, the residue was dissolved in chloroform, dried with Na_2SO_4, and taken to dryness to obtain the Schiff bases as yellow oils. They were used for complex formation without further purification. The preparation of the solid tetradentate ligands H_2B^1, H_2B^2, and H_2B^3 according to eq 7b was described recently.[9]

Complexes. Complexes Ni(*t*-BuMesal-H)$_2$, Ni(*t*-BuMesal-Me)$_2$, and Ni(*t*-BuMesal-Et)$_2$ were prepared in a one-pot reaction by adding an excess of an aqueous solution of the amine (NH_3, $MeNH_2$, and $EtNH_2$, respectively), 5 mmol of $Ni(CH_3COO)_2{\cdot}4H_2O$, and 10 mmol of sodium acetate to the solution of 10 mmol of H-*t*-BuMesal in 60 mL of ethanol, refluxing, and cooling, whereupon crystallization occurred. The same procedure was applied for the preparation of Ni(NO_2Mesal-R)$_2$ (R = Et, *i*-Pr), Ni(BrMesal-R)$_2$ (R = Et, *i*-Pr), Zn(*t*-BuMesal-Et)$_2$, and Zn(*i*-PrHsal-Et)$_2$ from the corresponding salicylaldehydes, amines, and metal salts, with methanol being the solvent.

The general route leading to complexes Ni(*t*-BuMesal-R)$_2$ (R = *n*-Pr, *i*-Pr, *n*-Bu, *i*-Bu, *t*-Bu, *neo*-Pe), Ni(*i*-BuHsal-R)$_2$ (R = Et, *i*-Pr), and Ni(*i*-PrHsal-R)$_2$ (R = Et, *i*-Pr) was the following. A solution of 20 mmol of the corresponding Schiff base H-XYsal-R, 10 mmol of $NiBr_2$, and 100 mmol of Et_3N in 100 mL of acetonitrile was mildly refluxed for 2−3 days, cooled, and filtered. The filtrate was taken to dryness and the residue was extracted with cyclohexane or petroleum ether (bp 40−80 °C), which was then dried with Na_2SO_4 and cooled for crystallization of the complex. Petroleum ether was used for recrystallization, with *tert*-butylamine being added in the case of Ni(*t*-BuMesal-*t*-Bu)$_2$.

The mixed complex [Ni(*t*-BuMesal-Et)$_2$][Zn(*t*-BuMesal-Et)$_2$]$_3$ was obtained by slow evaporation of an acetone solution of 0.2 mmol of Ni(*t*-BuMesal-Et)$_2$ and 0.8 mmol of Zn(*t*-BuMesal-Et)$_2$ at ambient temperature. The residue consisted of brownish crystals of the mixed complex (main component) and, as impurity, yellowish crystals of excess Zn(*t*-BuMesal-Et)$_2$, which were separated under the microscope.

(11) Sacconi, L. *Transition Metal Chemistry*; Marcel Dekker, Inc.: New York, 1968; Vol. 4.
(12) Ligett, R. W.; Diehl, H. *Proc. Iowa Acad. Sci.* **1945**, *52*, 191.
(13) Casiraghi, G.; Casuati, G.; Puglia, G.; Sartori, G.; Terenghi, G. *J. Chem. Soc., Perkin Trans. I* **1980**, 1862.
(14) Borsche, W. *Chem. Ber.* **1917**, *50*, 1339.
(15) Schotten, C. *Chem. Ber.* **1878**, *11*, 784.
(16) Adams, R. *J. Am. Chem. Soc.* **1919**, *41*, 268.

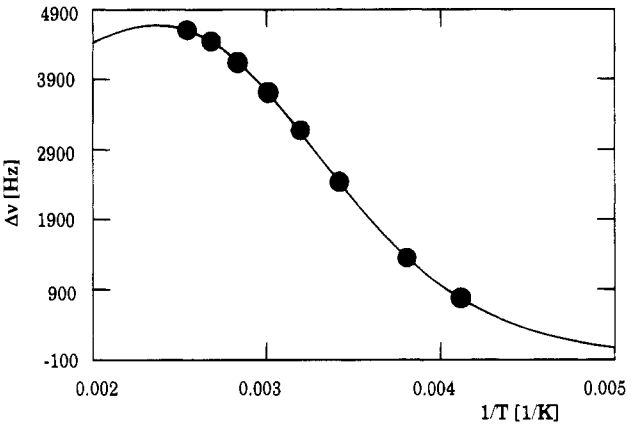

Figure 1. Temperature dependence of the chemical shift of the 4-H resonance for the complex Ni(*t*-BuMesal-Et)$_2$ in $C_2D_2Cl_4$.

The ratio Zn/Ni in the mixed complex was found to be 3:1 by X-ray fluorescence analysis.

The results of elemental analysis were in good agreement with the calculated data (see Table S1 in the supporting information).

Instrumentation. UV/vis spectra: diode array spectrophotometer (Hewlett-Packard, type 8451A). Near-IR spectra: double beam spectrophotometer (Zeiss, type DMR-21). ^{1}H NMR spectra: FT-NMR spectrometer (Bruker, type AC 300, 300 MHz). Magnetic susceptibility: magnetic susceptibility balance (Johnson–Matthey, type MSB-MKI). Slow kinetics: double beam spectrophotometer (Perkin-Elmer, type 554). Fast kinetics: modified[5a] stopped-flow spectrophotometer (Durrum, D 110).

Equilibrium Constants for Adduct Formation. Equilibrium constants K_1 and K_2 for pyridine addition according to eq 4 were determined by spectrophotometric titration. The Abs/[py] data (Abs = absorbance) were computer-fitted to eq 8.[1] The symbols Abs(NiA$_2$), Abs(NiA$_2$·py), and Abs(NiA$_2$·2py) refer to the absorbance of the three species involved at $[Ni]_{tot}$.

$$\text{Abs} = \frac{\text{Abs}(NiA_2) + \text{Abs}(NiA_2{\cdot}py)K_1[py] + \text{Abs}(NiA_2{\cdot}2py)K_1K_2[py]^2}{1 + K_1[py] + K_1K_2[py]^2} \quad (8)$$

^{1}H NMR Measurements. The details of the ^{1}H NMR investigation of the configurational equilibrium eq 5 have been described recently.[4] The spectra of complexes Ni(XYsal-R)$_2$ in $C_2D_2Cl_4$ were recorded in the temperature range 233–393 K (standard $(CH_3)_4Si$). In the case of Ni(*t*-BuMesal-*n*-Pr)$_2$ the solvent was acetone-d_6 and the range was 193–313 K. The paramagnetic band shift, $\Delta\nu$, is a direct measure of the fraction of the tetrahedral (paramagnetic) isomer present in solution[4] and follows the relationships in eqs 9a and 9b. Least-squares fitting

$$\Delta\nu = \Delta\nu_{dia} + CT^{-1}K_{p,t}(1 + K_{p,t})^{-1} \quad (9a)$$

$$\Delta\nu = \Delta\nu_{dia} + CT^{-1}[\exp(\Delta H_{p,t}°/RT)\exp(-\Delta S_{p,t}°/R) + 1]^{-1} \quad (9b)$$

of eq 9b to the experimentally obtained data for $\Delta\nu(T)$ led to the parameters C, $\Delta H_{p,t}°$, and $\Delta S_{p,t}°$ (the value for $\Delta\nu_{dia}$ was taken from the diamagnetic reference complexes Zn(*t*-BuMesal-Et)$_2$ and Zn(*i*-PrHsal-Et)$_2$ or from the corresponding free ligands H-XYsal-R). For each complex, the evaluation of these parameters was done for the resonance signal of three to four different protons (preferentially: $-HC{=}N$; $-HC{=}NCH_2-$; aromatic 4-*H*, 5-*H*, or 6-*H*; 2-C(CH_3)$_3$; 5-CH_3), and the results were averaged. Figure 1 demonstrates the temperature dependence of the 4-H resonance for the complex Ni(*t*-BuMesal-Et)$_2$.

Kinetic Measurements. Reaction 6 was followed by conventional spectrophotometry (slow substitution) or by stopped-flow spectrophotometry (fast substitution) under pseudo-first-order conditions (at least 10-fold excess of H_2B) at a suitable wavelength in the range 440–710 nm. Equation 10 (irreversible first-order reaction) was computer-fitted to the Abs/*t* data obtained. Some experiments were carried out under

$$\text{Abs} = (\text{Abs}_0 - \text{Abs}_\infty)[\exp(-k_{obsd}t)] + \text{Abs}_\infty \quad (10)$$

stoichiometric conditions ([complex] = [H_2B]), and eq 11 (irreversible second-order reaction) was fitted to the data. The programs used were based on the least-squares method.

$$\text{Abs} = \text{Abs}_\infty + (\text{Abs}_0 - \text{Abs}_\infty)/(1 + [\text{complex}]_0kt) \quad (11)$$

Table 1. Crystallographic Data for Complexes Ni(*t*-BuMesal-Et)$_2$ and Zn(*t*-BuMesal-Et)$_2$

	[Ni(*t*-BuMesal-Et)$_2$]	Zn(*t*-BuMesal-Et)$_2$]
chemical formula	$C_{28}H_{40}N_2O_2Ni$	$C_{28}H_{40}N_2O_2Zn$
form wt, g mol^{-1}	495.35	502.01
space group	$P2_1/c$	$C2/c$
a, Å	12.188(4)	27.14(2)
b, Å	11.455(4)	13.17(1)
c, Å	18.852(6)	18.30(2)
β, deg	97.66(1)	120.64(2)
V, Å^3	2609(2)	5627(10)
Z	4	8
T, °C	24	23
ϱ(calcd), g cm^{-3}	1.27	1.19
μ, cm^{-1}	7.78	8.91
R (F_o)[a]	0.0406	0.0395
R_w(F_o)[b]	0.0367	0.0357

[a] $R(F_o) = \sum(|F_o| - |F_c|)/\sum|F_o|$. [b] $R_w(F_o) = \sum w^{1/2}(F_o - F_c)/\sum w^{1/2}F_o$.

Table 2. Atomic Parameters for the Coordination Core of Complexes Ni(*t*-BuMesal-Et)$_2$ and Zn(*t*-BuMesal-Et)$_2$

atom	*x*/*a*	*y*/*b*	*z*/*c*	U_{eq}[a]
		Ni(*t*-BuMesal-Et)$_2$		
Ni1	0.4068(0)	0.0140(0)	0.2882(0)	0.0367(02)
O1	0.2717(1)	0.0213(1)	0.2294(1)	0.0416(10)
N1	0.4814(2)	−0.0457(2)	0.2133(1)	0.0387(12)
O2	0.5433(1)	0.0484(1)	0.3396(1)	0.0421(09)
N2	0.3313(2)	0.0289(2)	0.3692(1)	0.0421(13)
		Zn(*t*-BuMesal-Et)$_2$		
Zn1	0.2764(0)	0.5057(0)	0.2371(0)	0.0479(02)
O1	0.2030(1)	0.4770(2)	0.2226(1)	0.0421(14)
N1	0.3204(1)	0.4670(2)	0.3596(2)	0.0551(19)
O2	0.3102(1)	0.4544(2)	0.1752(1)	0.0573(15)
N2	0.2796(1)	0.6507(2)	0.2087(2)	0.0619(20)

[a] $U_{eq} = {}^1/_3(U_{11} + U_{22} + U_{33})$.

X-ray Structure Determination. Crystals of Ni(*t*-BuMesal-Et)$_2$ (greenish brown) and Zn(*t*-BuMesal-Et)$_2$ (pale yellow) were grown as short prisms from petroleum ether and methanol, respectively. The crystals chosen for X-ray measurements had the dimensions 0.16 × 0.45 × 0.7 mm (Ni(*t*-BuMesal-Et)$_2$) and 0.32 × 0.35 × 1.0 mm (Zn(*t*-BuMesal-Et)$_2$). Intensities were measured on a four-circle diffractometer (Stoe-Stadi-4) using graphite-monochromatized Mo Kα radiation (λ = 0.71069 Å; scan $2\theta{:}\omega$ = 1:1). Cell constants were determined on the same instrument by the least-squares method from the 2θ angles of 66 (Ni(*t*-BuMesal-Et)$_2$, T = 296 K) and 48 reflections (Zn(*t*-BuMesal-Et)$_2$, T = 295 K), respectively. LP and background corrections and a numerical absorption correction (SHELX-76) were applied.

The structure was solved by direct methods with SHELXS-86 and refined by least-squares to the R values given in Table 1. Hydrogen atoms were positioned geometrically (C–H distance = 1.08 Å) and not refined. An empirical extinction correction was applied. All crystallographic calculations were performed with the programs SHELX-76 and SHELXS-86 on an IBM 3081K computer at the Technische Hochschule Darmstadt. Scattering factors f_o, f' and f'' for C, H, N, and O are stored in SHELX-76. The final positional parameters are given in Table 2. (Data for Ni and Zn were taken from *International Tables for X-ray Crystallography*; Kynoch Press: Birmingham, England, 1974; Vol. IV.)

Table 3. Visible and Near-IR Absorption [λ_{max}, nm (ϵ_{max}, M^{-1} cm^{-1})] of Complexes Ni(XYsal-R)$_2$ in Acetone (visible) and Carbon Tetrachloride (Near-IR) and Magnetic Moments at 298 K

complex	visible	near-IR	μ_{eff}, μ_B
Ni(*t*-BuMesal-H)$_2$	420 (5200), 438s (4530), 570 (126)		<0.2
Ni(*t*-BuMesal-Me)$_2$	396 (4720), 410s (4580), 654 (169)	1400 (7.5)	<0.2
Ni(*t*-BuMesal-Et)$_2$	384 (6720), 424s (4190), 660 (130)	1410 (28)	<0.2
Ni(*t*-BuMesal-*n*-Pr)$_2$	388 (5800), 420s (4580), 652 (139)	1410 (14)	<0.2
Ni(*t*-BuMesal-*i*-Pr)$_2$	382 (10280), 430s (4270), 586s (148), 708 (96)	1520 (71)	3.21
Ni(*t*-BuMesal-*n*-Bu)$_2$	390 (5440), 418s (4470), 654 (145)	1400 (19)	3.19
Ni(*t*-BuMesal-*t*-Bu)$_2$	396 (5320), 416s (4810), 648 (165)	1410 (11)	<0.2
Ni(*t*-BuMesal-*t*-Bu)$_2$	382 (10700), 428s (5280), 548 (291), 604s (186), 712 (66)	1700 (45)	3.21
Ni(*t*-BuMesal-*neo*-Pe)$_2$	398 (5760), 420s (4680), 642s (145)	*a*	0.86
Ni(*i*-PrHsal-Et)$_2$	412 (5030), 518s (115), 632 (95)	*a*	<0.2
Ni(*i*-PrHsal-*i*-Pr)$_2$	368 (8420), 412s (4095), 510s (192), 578s (116), 700 (76)	*a*	3.35
Ni(*i*-BuHsal-Et)$_2$	414 (4560), 512s (113), 636 (83)	*a*	<0.2
Ni(*i*-BuHsal-*i*-Pr)$_2$	370 (7370), 412s (3540), 516s (197), 572s (124), 702 (82)	*a*	3.33
Ni(NO_2Mesal-Et)$_2$	430 (10790), 606 (89)	*a*	<0.2
Ni(NO_2Mesal-*i*-Pr)$_2$	422 (11310), 608s (74), 700s (41)	*a*	3.06
Ni(BrMesal-Et)$_2$	418 (5220), 620 (135)	*a*	<0.2
Ni(BrMesal-*i*-Pr)$_2$	382 (7720), 418s (5050), 514s (194), 602s (99), 686s (63)	*a*	<0.2
Ni(*t*-BuMesal-Et)$_2$/Zn(*t*-BuMesal-Et)$_2$ (1:3)	*a*	*a*	≈0.8
Ni(salen)	412 (6660), 450s (3160), 550s (160)	*a*	<0.2
Ni(salpn)	416 (5070), 710s (67)	*a*	1.64
Ni(sal(Me)$_2$en)	412 (6850), 442s (3690), 546s (158)	*a*	<0.2

[a] Not studied.

Results

Visible/Near-IR Absorption and Magnetic Properties of the Complexes. The characteristics of the visible spectra in acetone and of the near-IR spectra in CCl_4 are compiled in Table 3.

The visible and near-IR absorptions of planar and tetrahedral nickel(II) complexes have been discussed in detail.[17] Complexes Ni(XYsal-R)$_2$ are generally characterized by a strong, weakly substituent-dependent absorption at 390 ± 20 nm ($\epsilon \approx 5200-11500$) and a shoulder at ≈420 nm ($\epsilon \approx 3500-5000$), which can be attributed to a MLCT overlapped by the "phenolate band" ($n \rightarrow \pi^*$ transition).[12,21] The most characteristic "planar" band is the one at 630−650 nm ($\epsilon \approx 100-170$).[2b] The tetrahedral or tetrahedrally distorted complexes Ni(XYsal-R)$_2$ have a band at 700−710 nm ($\epsilon \approx 70-100$), a shoulder at 570−600 nm ($\epsilon \approx 100-150$), and, most typically, a weak near-IR band ($\epsilon \approx 10-70$) at 1400−1700 nm. With regard to the distortion effect of the alkyl group R in complexes Ni(*t*-BuMesal-R)$_2$, the sum of the spectral data and the relative intensities of the various absorptions lead to the qualitative order below (12).

$$\text{Me} \ll n\text{-Pr}, n\text{-Bu}, i\text{-Bu}, neo\text{-Pe} < \text{Et} < i\text{-Pr} < t\text{-Bu} \quad (12)$$
$$\text{increasing tetrahedral distortion} \longrightarrow$$

The coordination geometry in Ni(*t*-BuMesal-R)$_2$ is most planar for R = Me and most tetrahedral for R = *t*-Bu. The equilibrium planar ⇌ tetrahedral is reversibly temperature dependent and shifted toward the tetrahedral isomer with increasing temperature. This is demonstrated in Figure 2 by the visible spectra of the most planar complex Ni(*t*-BuMesal-Me)$_2$, recorded in the temperature range 20−70 °C. The typical "planar" band at 650 nm decreases with increasing temperature.

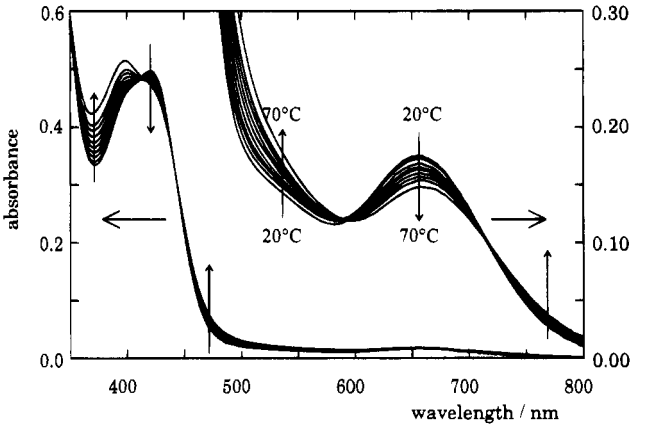

Figure 2. Visible spectra of the complex Ni(*t*-BuMesal-Me)$_2$ in toluene in the temperature range 20−70 °C.

Analyzing the solid state magnetic moments (Table 3), one has to keep in mind that magnetic moments of about 3 μ_B can indicate tetrahedral as well as octahedral coordination. The magnetic moments have to be discussed therefore in combination with the corresponding visible and near-IR absorption spectra. The experimental magnetic moment of 3.21 μ_B, as found for complexes Ni(*t*-BuMesal-R)$_2$ with R = *i*-Pr and R = *t*-Bu, is in agreement with tetrahedral coordination. The visible spectrum of Ni(*t*-BuMesal-*n*Bu)$_2$ (Table 3) clearly points to planar coordination. The magnetic moment of 3.19 μ_B for this complex seems thus to be due to octahedral coordination, resulting from Ni−O interactions between neighboring molecules in the lattice. Partial octahedral coordination of this type might also explain the magnetic moment 0.86 μ_B, as found for the complex Ni(*t*-BuMesal-*neo*-Pe)$_2$ which, according to its visible spectrum, is predominantly planar. The magnetic moments of 3.35, 3.33, and 3.06 μ_B, obtained for complexes Ni(*i*-PrHsal-*i*-Pr)$_2$, Ni(*i*-BuHsal-*i*-Pr)$_2$, and Ni(NO_2Mesal-*i*-Pr)$_2$, respectively, obviously indicate tetrahedral coordination. The

(17) For tetrahedral nickel(II) complexes one expects three typical transitions[18] at 2500−1400 nm ($\epsilon \approx 10-50$), at 1400−900 nm ($\epsilon \approx 100-200$), and at 660−500 nm ($\epsilon \approx 200-500$). As in the case of Ni(sal-*i*-Pr)$_2$,[19] the latter absorption is often structured. Three spin-allowed transitions in the range 700−400 nm ($\epsilon \approx 50-200$) are typically found for planar four-coordinate nickel(II) complexes, albeit mostly not well resolved and partially covered by CT bands. As a result, one often observes just one band, especially in the case of σ-donating ligands with weak π-acceptor properties.[20] The most characteristic indication for tetrahedral coordination is thus the occurrence of absorption bands in the near-IR range.

(18) Wilkinson, G., Gillard, R. D., McCleverty, J. A., Eds. *Comprehensive Coordination Chemistry*; Pergamon-Press: Oxford, 1987; Vol. 5.
(19) Cruse, D. A.; Gerloch, M. *J. Chem. Soc., Dalton Trans.* **1977**, 152.
(20) Nishida, Y., Kida, S. *Coord. Chem. Rev.* **1979**, *27*, 275.
(21) Becker, M.; Elias, H. *Inorg. Chim. Acta* **1986**, *116*, 47.

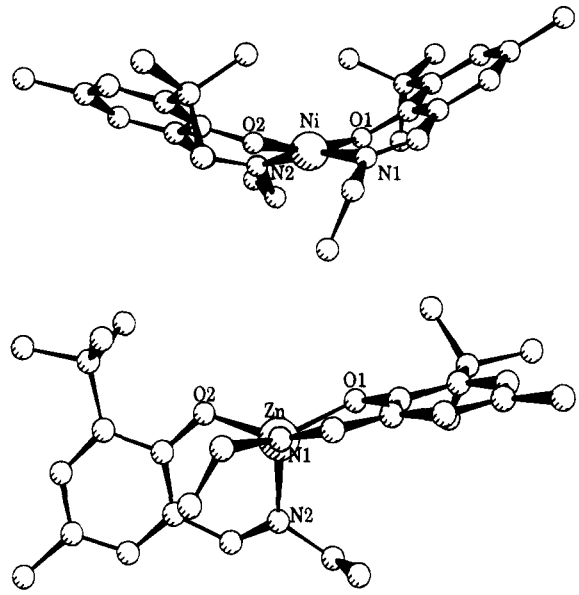

Figure 3. View of the coordination geometry in the complexes Ni(*t*-BuMesal-Et)$_2$ and Zn(*t*-BuMesal-Et)$_2$.

α-branched isopropyl group R, in combination with substituents X = isopropyl, isobutyl and NO_2, creates substantial steric congestion.

The magnetic moment of $\mu_{exp} \approx 0.8\ \mu_B$ found for the mixed complex [Ni(*t*-BuMesal-Et)$_2$][Zn(*t*-BuMesal-Et)$_2$]$_3$ is an interesting result. It demonstrates that, imbedded into the host lattice of tetrahedral Zn(*t*-BuMesal-Et)$_2$, the planar (diamagnetic) nickel complex becomes tetrahedral and thus paramagnetic. This finding indicates that the energy difference between planar and tetrahedral Ni(*t*-BuMesal-Et)$_2$ is obviously rather small. Chakravorty[22] reported the same effect for planar Ni(5-Mesal-*i*-Pr)$_2$ imbedded into tetrahedral Zn(5-Mesal-*i*-Pr)$_2$.

Structure of Complexes Ni(*t*-BuMesal-Et)$_2$ and Zn(*t*-BuMesal-Et)$_2$. Figure 3 gives a view of the coordination geometry in Ni(*t*-BuMesal-Et)$_2$ and Zn(*t*-BuMesal-Et)$_2$. The nickel coordinates the ligands in a basically planar fashion with a trans-N_2O_2 arrangement of the donor atoms. Both ligands are bent off the coordination plane. The donor atom arrangement is not strictly planar but tetrahedrally distorted (dihedral angle $\theta = 21.7°$). The Ni−O and Ni−N distances (mean: 1.856 and 1.899 Å, respectively; Table 4) are normal in the sense that they are very close to those of the planar complex Ni(sal-Et)$_2$.[23] The shortest intermolecular Ni−O distance is 5.92 Å, which excludes additional Ni−O bonding between neighboring complex units.

The view of the analogous zinc complex Zn(*t*-BuMesal-Et)$_2$ (Figure 3) clearly demonstrates the expected tetrahedral coordination. The angles listed in Table 4 confirm the tetrahedral arrangement of the donor atoms around the zinc, although there are small deviations from the theoretical value of 109°. The Zn−O and Zn−N distances (mean: 1.907 and 1.995 Å, respectively) are significantly longer than the corresponding distances in the nickel complex. This is in line with the general observation that the M−O and M−N distances in complexes M(sal-R)$_2$ are longer when the two salicylaldimines are tetrahedrally coordinated instead of planar.[25]

(22) Chakravorty, A. *Inorg. Chem.* **1965**, *4*, 127.
(23) For Ni(sal-Et)$_2$ the mean Ni−O and Ni−N distances are 1.84 and 1.92 Å, respectively.[24]
(24) Shkol'nikova, L. M.; Knyazeva, A. N.; Voblikova, V. A. *J. Struct. Chem.* **1967**, *8*, 77.
(25) For the tetrahedrally distorted complex Ni(sal-*i*-Pr)$_2$, it is reported,[26] for example, that d(Ni−O) = 1.896 Å and d(Ni−N) = 1.970 Å.

Table 4. Selected Distances (Å) and Bond Angles (deg) for Complexes Ni(*t*-BuMesal-Et)$_2$ and Zn(*t*-BuMesal-Et)$_2$

[Ni(*t*-BuMesal-Et)$_2$]		[Zn(*t*-BuMesal-Et)$_2$]	
	Distances		
Ni−O1	1.861(2)	Zn−O1	1.906(2)
Ni−O2	1.852(2)	Zn−O2	1.907(2)
Ni−N1	1.905(2)	Zn−N1	1.997(3)
Ni−N2	1.893(2)	Zn−N2	1.992(3)
Ni−O[a]	5.92	Zn−O[a]	6.92
	Angles		
O1−Ni−N1	92.7(1)	O1−Zn−N1	95.2(1)
O1−Ni−N2	89.4(1)	O1−Zn−N2	109.6(1)
O2−Ni−N2	93.3(1)	O2−Zn−N2	95.0(1)
N1−Ni−O2	88.9(1)	N1−Zn−O2	112.4(1)
O1−Ni−O2	164.6(1)	O1−Zn−O2	129.1(1)
N1−Ni−N2	164.1(1)	N1−Zn−N2	117(1)

[a] Shortest distance to O of neighboring complex unit.

Adduct Formation with Pyridine. The equilibrium constants K_1 and K_2 for adduct formation with pyridine according to eq 4 are summarized in Table 5. As a general result, it is found that $K_1 \ll K_2$, which is in agreement with earlier results obtained for similar systems.[1,4,27] Compared to that of the five-coordinate mono adduct, formation of the octahedral bis adduct is thus much more favored, with K_2/K_1 ranging from 1.9 to 3000. The size of both K_2/K_1 and $\beta = K_1K_2$ is obviously controlled by steric and electronic factors. In the case of complexes Ni(*t*-BuMesal-R)$_2$, the effect of R on β (and K_1, respectively) is mainly steric and follows sequence below (13). As a consequence of the steric demands of R, the formation of the

$$t\text{-Bu, } neo\text{-Pe} \ll i\text{-Pr} < i\text{-Bu} < n\text{-Pr} \approx n\text{-Bu} < \text{Et} \ll \text{Me} \qquad (13)$$
$$\text{increasing } \beta$$

octahedral adduct is hindered by either tetrahedral distortion or shielding of the metal center. The alkyl group R = *neo*-Pe is a good example for the latter effect. Although Ni(*t*-BuMesal-*neo*-Pe)$_2$, according to sequence 12, is not strongly distorted, the neopentyl groups block the addition of pyridine completely. The extremely high value of $K_2/K_1 = 3000$ found for R = *i*-Pr seems to indicate that only the addition of the second pyridine molecule (i.e., formation of the octahedral bis adduct) is energetically favorable enough to overcome the distortion in Ni(*t*-BuMesal-*i*-Pr)$_2$.

The high β values obtained for Ni(BrMesal-Et)$_2$ and Ni(BrMesal-*i*-Pr)$_2$ reflect the electron-withdrawing properties of the bromine substituent in the 3-position, which makes the nickel a better Lewis acid. The fact that β(Et) < β(*i*-Pr) is somewhat surprising though and is not in line with the effect of R in complexes Ni(*t*-BuMesal-R)$_2$.

Configurational Equilibrium Planar ⇌ Tetrahedral. The results obtained from the temperature dependence of the chemical shift of the various protons in complexes Ni(XYsal-R)$_2$ are summarized in Table 6. The enthalpy of isomerization, ranging from about 18 to 28 kJ mol^{-1}, is in all cases positive, which means that the planar structure is energetically favored. The effect of X and R on $\Delta H_{p,t}°$ is relatively small. The observed changes in $\Delta G_{p,t}°$ and $K_{p,t}$, respectively, are more affected by changes in the entropy of isomerization, which ranges from about 19 to 69 J/(mol K). Large positive values of $\Delta S_{p,t}°$ increase the size of the equilibrium constant $K_{p,t}$, i.e., they favor the tetrahedral isomer. The lowest values for $K_{p,t}$, 0.004 and 0.005, are found for complexes Ni(*i*-PrHsal-Et)$_2$ and Ni(sal-Et)$_2$. The highest values of 0.31 and 0.17 are obtained for complexes Ni(*t*-BuMesal-Et)$_2$ and Ni(*t*-BuMesal-*n*-Bu)$_2$,

Table 5. Equilibrium Constants for the Addition of Pyridine to Complexes [Ni(XYsal-R)$_2$] in Acetone According to Eq 4 at 298 K

X	Y	Re	K_1, M^{-1}	K_2, M^{-1}	$\beta = K_1K_2$, M^{-2}	K_2/K_1
t-Bu	Me	Me	28.8 ± 5.3	53.5 ± 9.9	1540 ± 280	1.85
t-Bu	Me	Et	4.15 ± 0.26	17.8 ± 2.7	73.8 ± 9.7	4.29
t-Bu	Me	*n*-Pr	1.33 ± 0.12	25.7 ± 1.3	34.2 ± 1.5	19.2
t-Bu	Me	*i*-Pr	0.03 ± 0.01	90.4 ± 22.9	2.49 ± 0.48	3000
t-Bu	Me	*n*-Bu	1.71 ± 0.09	21.7 ± 1.1	37.1 ± 1.5	12.7
t-Bu	Me	*i*-Bu	0.41 ± 0.02	40.3 ± 0.8	16.5 ± 0.3	98.3
t-Bu	Me	*t*-Bu				*a*
t-Bu	Me	*neo*-Pe				*a*
t-Bu	H	Et	0.53 ± 0.02	239 ± 12	127 ± 3	450
i-Bu	H	*i*-Pr	0.25 ± 0.08	377 ± 38	94.7 ± 10.5	1510
i-Pr	H	Et	0.44 ± 0.02	190 ± 19	84.4 ± 2.6	432
i-Pr	H	*i*-Pr	1.52 ± 0.17	30.9 ± 3.1	47.2 ± 6.5	20.3
Br	Me	Et	14.3 ± 3.4	498 ± 50	7104 ± 50	34.8
Br	Me	*i*-Pr	77.5 ± 4.8	220 ± 22	17100 ± 200	2.84

[a] Addition of pyridine not observed.

Table 6. Thermodynamic Parameters Describing the Configurational Equilibrium Planar ⇌ Tetrahedral of Several Complexes Ni(XYsal-R)$_2$ in $C_2D_2Cl_4$[a]

X	Y	R	$\Delta H_{p,t}°$, kJ/mol	$\Delta S_{p,t}°$, J/(mol K)	$\Delta G_{p,t}°$(298), kJ/mol	$K_{p,t}$(298)
H	H	Et	17.7 ± 0.6	19.1 ± 2.1	12.0 ± 2.4	0.005 ± 0.002
t-Bu	Me	Et	19.6 ± 5.0	59 ± 17	1.92 ± 0.42	0.31 ± 0.06
t-Bu	Me	*n*-Bu	20.5 ± 2.0	59.8 ± 7.1	3.86 ± 0.60	0.17 ± 0.03
t-Bu	Me	*i*-Bu	21.3 ± 2.3	53.2 ± 8.6	5.4 ± 1.2	0.09 ± 0.02
t-Bu	Me	*neo*-Pe	23.1 ± 8.6	55 ± 34	6.7 ± 1.8	0.06 ± 0.02
t-Bu	Me	*t*-Pr				≫1[b]
t-Bu	Me	*t*-Bu				≫1[b]
i-Pr	H	Et	21.6 ± 0.8	68.9 ± 4.9	13.7 ± 2.8	0.004 ± 0.001
i-Bu	H	Et	28.4 ± 3.5	69 ± 14	7.9 ± 1.6	0.04 ± 0.01

[a] Deuterated 1,1,2,2-tetrachloroethane. [b] Complex is predominantly tetrahedral in the temperature range studied. Due to $K_{p,t} \gg 1$, relationship 9a takes the form $\Delta\nu = \Delta\nu_{dia} + C/T$ (Curie behavior).

respectively. One should keep in mind, however, that complexes Ni(*t*-BuMesal-*i*-Pr)$_2$ and Ni(*t*-BuMesal-*t*-Bu)$_2$ are the most tetrahedral ones within the series Ni(*t*-BuMesal-*R*)$_2$ studied. For these two complexes, $K_{p,t} \gg 1$, so that relationships 9a and 9b are no longer useful for the determination of $K_{p,t}$ (see Table 6).

The overall result for complexes Ni(*t*-BuMesal-R)$_2$ is that the organic group R increases the size of $K_{p,t}$ according to

$$\underset{\text{increasing } K_{p,t}}{\xrightarrow{\textit{neo}\text{-Pe} < i\text{-Bu} < n\text{-Bu} < \text{Et} \ll i\text{-Pr}, t\text{-Bu}}} \quad (14)$$

sequence 14. This sequence parallels the qualitative order 12, as derived from the visible absorption spectra.

Kinetic Results. Ligand substitution according to eq 6, as studied under pseudo-first-order conditions with an excess of H_2B, is an irreversible first-order reaction. The change in absorbance with time can be fitted to the exponential function of eq 10, which leads to the experimental rate constant k_{obsd}. The plot of k_{obsd} versus [H_2B] is linear (see, for example, Figure 4), with a very small intercept in some cases. The rate of ligand substitution is therefore described by eq 15. The second-order rate constants k_{H_2B}

$$\text{rate} = k_{obsd}[\text{complex}] = (k_s + k_{H_2B}[H_2B])[\text{complex}] \approx k_{H_2B}[H_2B][\text{complex}] \quad (15)$$

(and first-order rate constants k_s) are compiled in Table 7. The size of rate constant k_{H_2B} is controlled by the specific combination of X substituent plus R group and covers almost 7 orders of magnitude for H_2B = H_2salen. For a given complex such as Ni(*t*-BuMesal-Et)$_2$, the attacking ligand H_2B affects the rate according to $k(H_2B^1):k(H_2B^2):k(H_2B^3)$ = 1:0.91:0.0031. Compared to H_2salen, the two methyl groups on the ethylene bridge in H_2B^3 reduce the rate of substitution by a factor of 326. As stated above, a small first-order rate constant k_s is observed in a few cases, which points to an additional, ligand-independent reaction channel.[28] The contribution of the term k_s[complex] to the overall rate (see rate law, eq 15) is negligibly small though.

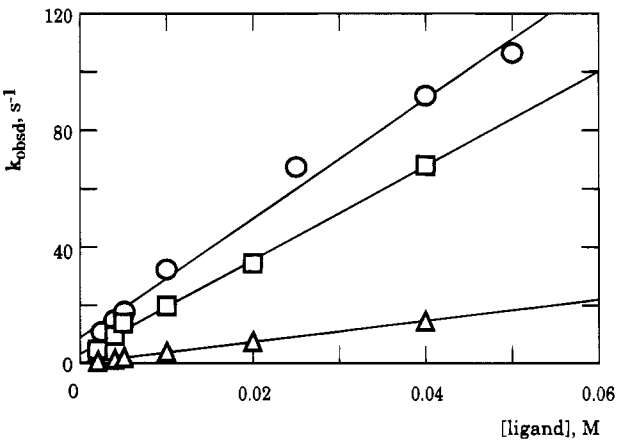

Figure 4. Plot of the experimental rate constant k_{obsd} for the reaction of Ni(*t*-BuMesal-Et)$_2$ (○), Ni(*t*-BuMesal-*n*-Bu)$_2$ (□), and Ni(*t*-BuMesal-*i*-Bu)$_2$ (△) with an excess of H_2salen in acetone at 298 K.

(26) Fox, M. R.; Orioli, P. L.; Lingafelter, E. C.; Sacconi, L. *Acta Crystallogr.* **1964**, *17*, 1159.
(27) (a) Jäger, E. G.; Kirchhof, B.; Schmidt, E.; Rende, B.; Kipke, A.; Müller, R. *Z. Anorg. Allg. Chem.* **1982**, *485*, 141. (b) Dakternieks, D. R.; Graddon, D. P.; Lindoy, L. F.; Mockler, G. M. *Inorg. Chim. Acta* **1973**, *7*, 467. (c) Graddon, D. P. *Coord. Chem. Rev.* **1969**, *4*, 1.
(28) The aprotic solvent acetone is obviously not able to open a solvent-initiated, ligand-independent reaction channel. The very small and not very reproducible k_s values obtained are probably due to protic trace impurities such as residual water or alcohol. Addition of small amounts of water increases the size of k_s, but the reactions still proceed to completion.

Table 7. Rate Constants for the Reaction of Complexes [Ni(XYsal-R)$_2$] with Ligands H_2B in Acetone According to Eq 6 at 298 K

X	Y	R	H_2B	k_{H_2B}, M^{-1} s^{-1}	k_s, s^{-1}
t-Bu	Me	H	H_2salen	$(2.5 \pm 0.1) \times 10^{-2}$	$(3.5 \pm 4.5) \times 10^{-5}$
t-Bu	Me	Me	H_2salen	37500 ± 400	
t-Bu	Me	Et	H_2salen	2050 ± 100	8.7 ± 2.6
t-Bu	Me	*n*-Pr	H_2salen	1860 ± 50	1.8 ± 1.4
t-Bu	Me	*i*-Pr	H_2salen	126 ± 4	0.16 ± 0.09
t-Bu	Me	*n*-Bu	H_2salen	1610 ± 50	3.2 ± 1
t-Bu	Me	*i*-Bu	H_2salen	364 ± 3	
t-Bu	Me	*t*-Bu	H_2salen	$(4.4 \pm 0.5) \times 10^{-3}$	
t-Bu	Me	*neo*-Pe	H_2salen	$\leq 10^{-3}$	
i-Pr	H	Et	H_2salen	113 ± 2	0.006 ± 0.011
i-Pr	H	*i*-Pr	H_2salen	76.3 ± 1.0	0.003 ± 0.005
i-Bu	H	Et	H_2salen	116 ± 1	
i-Bu	H	*i*-Pr	H_2salen	78.1 ± 0.3	
Br	Me	Et	H_2salen	74.6 ± 0.7	$(6 \pm 39) \times 10^{-4}$
Br	Me	*i*-Pr	H_2salen	132 ± 2	0.01 ± 0.01
NO_2	Me	Et	H_2salen	1190 ± 80	1.3 ± 0.5
NO_2	Me	*i*-Pr	H_2salen	1420 ± 250	0.30 ± 0.15
t-Bu	Me	Me	H_2salpren	32000 ± 2000	
t-Bu	Me	Et	H_2salpren	1870 ± 60	
t-Bu	Me	*n*-Pr	H_2salpren	1360 ± 30	
t-Bu	Me	*i*-Pr	H_2salpren	95.8 ± 3.3	
t-Bu	Me	*i*-Bu	H_2salpren	305 ± 6	
t-Bu	Me	Me	H_2sal(Me)$_2$en	132 ± 3	
t-Bu	Me	Et	H_2sal(Me)$_2$en	6.29 ± 0.16	
t-Bu	Me	*n*-Pr	H_2sal(Me)$_2$en	4.23 ± 0.17	$(5 \pm 32) \times 10^{-4}$
t-Bu	Me	*i*-Pr	H_2(sal(Me)$_2$en	0.29 ± 0.01	
t-Bu	Me	*n*-Bu	H_2sal(Me)$_2$en	4.56 ± 0.01	
t-Bu	Me	*i*-Bu	H_2sal(Me)$_2$en	0.68 ± 0.02	
i-Bu	H	Et	H_2sal(Me)$_2$en	0.46 ± 0.01	$(2.2 \pm 0.9) \times 10^{-4}$

Table 8. Activation Parameters for the Reaction of Complexes [Ni(XYsal-R)$_2$] with Ligands H_2B in Acetone According to Eq 6

X	Y	R	H_2B	$\Delta H^{\ddagger}$, kJ mol^{-1}	$\Delta S^{\ddagger}$, J mol^{-1} K^{-1}
t-Bu	Me	*n*-Pr	H_2salen	34.0 ± 2.8	-67.3 ± 4.7
t-Bu	Me	*i*-Pr	H_2salen	30.7 ± 2.9	-101 ± 10
t-Bu	Me	*n*-Bu	H_2salen	34.5 ± 0.2	-84.4 ± 0.5
t-Bu	Me	*i*-Bu	H_2salen	32.0 ± 2.5	-88.2 ± 6.6
i-Bu	H	Et	H_2salen	45.7 ± 1.4	-52.5 ± 1.7
i-Bu	H	*i*-Pr	H_2salen	36.7 ± 1.8	-85.9 ± 4.3
i-Pr	H	Et	H_2salen	43.4 ± 0.7	-59.9 ± 0.9
i-Pr	H	*i*-Pr	H_2salen	37.4 ± 0.8	-83.5 ± 1.3
Br	Me	Et	H_2salen	42.4 ± 0.8	-68.2 ± 1.3
Br	Me	*i*-Pr	H_2salen	29.2 ± 0.5	-107 ± 2
NO_2	Me	Et	H_2salen	19.9 ± 2.8	-115 ± 12
NO_2	Me	*i*-Pr	H_2salen	13.7 ± 1.5	-138 ± 12
t-Bu	Me	Me	H_2sal(Me)$_2$en	33.7 ± 0.7	-91.1 ± 1.8
t-Bu	Me	Et	H_2sal(Me)$_2$en	45.4 ± 2.5	-78.6 ± 2.3

Table 8 summarizes the data obtained for the activation parameters. It is important to note that the entropy of activation is in all cases negative. For the system Ni(NO_2Mesal-*i*-Pr)$_2$/H_2B[1], the enthalpy of activation is lowest (13.7 ± 1.5 kJ mol^{-1}) and the negative entropy of activation is highest (-138 J/(mol K)), whereas for the system Ni(*i*-BuHsal-Et)$_2$/H_2B[1] the opposite is found (45.7 ± 1.4 kJ mol^{-1} and -53 J/(mol K), respectively).

Discussion

It follows from the visible absorption spectra, magnetic moments, and temperature-dependent ^{1}H NMR spectra that specific combinations of X and R substituents force complexes Ni(XYsal-R)$_2$ to leave the preferred planar trans-N_2O_2 coordination geometry and become more or less tetrahedrally distorted. The magnetic moments of the solid complexes at 298 K reflect either planarity ($\mu < 0.2$ μ_B) or tetrahedral (octahedral) coordination ($\mu = 3.2-3.3$ μ_B). In solution, the variable degree of steric repulsion and tetrahedral distortion is more pronounced, as indicated by sequences 12, 13, and 14.[29] The complex Ni(*t*-BuMesal-Et)$_2$ can be taken as a typical example. According to the X-ray structure analysis, the trans-N_2O_2Ni coordination core is planar (albeit slightly distorted; see Figure 3), and the compound is therefore diamagnetic (Table 3). In acetone solution, however, this complex shows the characteristic "planar" absorption bands (Table 3) and adds pyridine to a much lesser extent than the corresponding planar complex with R = Me (Table 5); thus, the equilibrium constant $K_{p,t}$ amounts to 0.31 (Table 6).

The equilibrium constants for pyridine addition, K_1 and K_2, are useful parameters for understanding which species are the thermodynamically dominating ones in the series of fast coupled solution equilibria described by eq 16 (NiA_2 = Ni(XYsal-R)$_2$, t = tetrahedral, p = planar). In the case of Ni(*t*-BuMesal-*t*-Bu)$_2$, pyridine is not coordinated at all, which means that this complex is mainly tetrahedral. The opposite is true for the complex Ni(*t*-BuMesal-Me)$_2$, with the bis(pyridine) adduct dominating.

$$NiA_2(t) \overset{K_{p,t}^{-1}}{\rightleftharpoons} NiA_2(p) \overset{K_1}{\rightleftharpoons} NiA_2{\cdot}py \overset{K_2}{\rightleftharpoons} NiA_2{\cdot}2py \quad (16)$$

The information coming from the temperature-dependent ^{1}H NMR studies allows us to quantify the configurational equilibrium of eq 5. For complexes Ni(*t*-BuMesal-R)$_2$, the data obtained for $K_{p,t}$ range from $\gg 1$ (R = *t*-Bu, *i*-Pr) to 0.06 (R = *neo*-Pe). If the planar and tetrahedral configurational isomers differ in reactivity toward ligand substitution, one would expect that the rate of substitution depends on the parameter $K_{p,t}$. This was indeed found for complexes Ni(R_2-ati)$_2$[3] reacting according to eq 2.[4]

Figure 5 presents schematically the effect of the alkyl group R on the rate of reaction 6 for complexes Ni(*t*-BuMesal-R)$_2$.

(29) For experimental reasons, the absorption spectra were taken in acetone (visible), toluene (temperature dependence), and carbon tetrachloride (near-IR) and the ^{1}H NMR spectra were taken in 1,1,2,2-tetrachloroethane. The kinetic studies were carried out in acetone. In view of possible solvent effects, the visible spectra of Ni(*t*-BuMesal-*n*-Bu)$_2$ and Ni(*t*-BuMesal-*t*-Bu)$_2$ were taken in acetone, toluene, and 1,1,2,2-tetrachloroethane. It was found that, within the limits of error, the data for λ_{max} and ϵ_{max} were identical for all three solvents.

Scheme 1. Mechanism Suggested for Ligand Substitution According to Eq 6

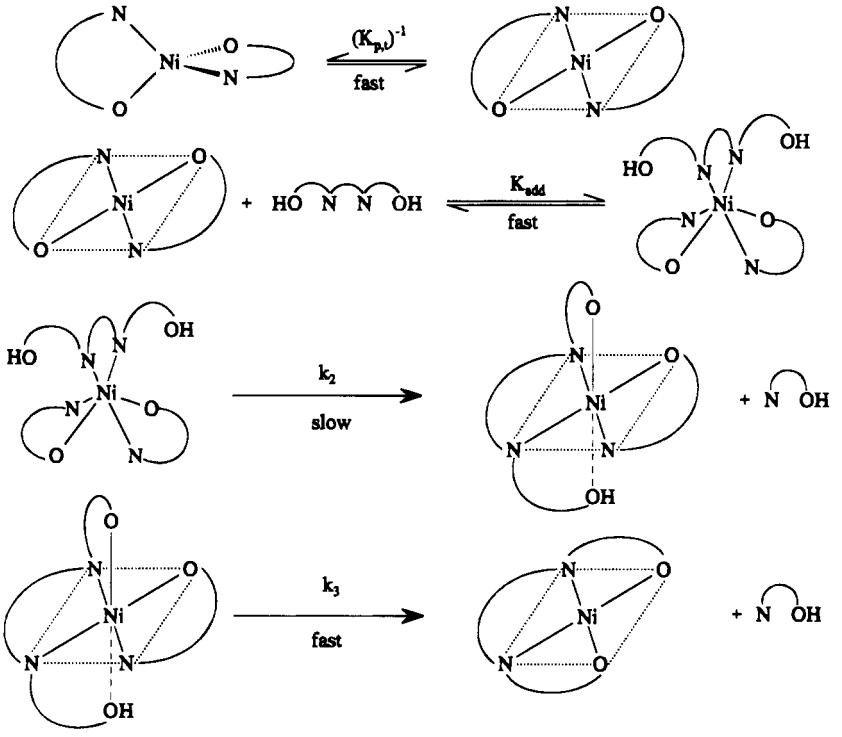

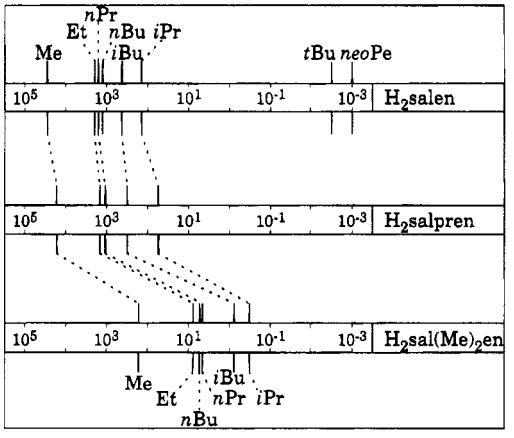

Figure 5. Schematic representation of rate constants k_{H_2B} (M^{-1} s^{-1}; 298 K) for the reaction of complexes Ni(*t*-BuMesal-R) according to eq 6.

For H_2B^1, the second-order rate constant k_{H_2B} spans from 3.75 $\times$ 10^4 M^{-1} s^{-1} for R = Me to 4.4 $\times$ 10^{-3} M^{-1} s^{-1} for R = *t*-Bu, which corresponds to a decrease in rate by almost 7 orders of magnitude. The R-dependent pattern of reactivity is the same for the attacking ligands H_2B^1, H_2B^2, and H_2B^3, the ligand H_2B^3 reacting considerably slower though. Despite the fact that, within the series Ni(*t*-BuMesal-R)$_2$, the slowest complex is the most tetrahedral one, it is obvious that the equilibrium planar $\rightleftharpoons$ tetrahedral cannot be the only rate-controlling factor.[30] The simple assumption that the rate constant k_{H_2B} decreases with increasing $K_{p,t}$ is disproved best by the complex Ni(*t*-BuMesal-*neo*-Pe)$_2$. Its reaction with H_2salen is extremely slow, although the absorption spectrum and the $K_{p,t}$ value of 0.06 point to essentially planar coordination geometry. An explanation for this low reactivity comes from the finding that the complex does not add pyridine at all. Although surrounded by a planar set of donor atoms, the nickel center is so much shielded by the neopentyl groups that the addition of pyridine is sterically blocked. With regard to ligand substitution, this would mean that nucleophilic addition of H_2salen to Ni(*t*-BuMesal-*neo*-Pe)$_2$ as the initiating step of ligand substitution is strongly hindered.

The results of the present study are thus in good agreement with the mechanism derived earlier for similar systems.[10] As shown in Scheme 1, the planar isomer of complexes Ni(XYsal-R)$_2$ equilibrates quickly with the attacking ligand H_2B to form a six-coordinate adduct in which H_2B is doubly N-coordinated.[10] This adduct splits off the first bidentate ligand in the rate-determining k_2 step, which includes proton transfer. The loss of the second bidentate ligand, the k_3 step, is a fast consecutive reaction which cannot be monitored in the present system.

Scheme 1 suggests that the experimental rate constant is a composite parameter, $k_{H_2B} = k_2(K_{p,t} + 1)^{-1}K_{add}$. Large values of $K_{p,t}$ exert thus a rate-reducing effect as well as small values of K_{add}. Small values of K_{add} result from sterically shielding groups R such as the neopentyl group and rigid attacking ligands such as H_2B^3. When $K_{p,t}$ is known, it should in principle be possible to determine K_{add} by studying eq 6 at high concentrations of H_2B and thus to obtain k_2.[31]

The activation parameters were determined from the temperature dependence of rate constant k_{H_2B}. As pointed out earlier, the entropy of activation is in all cases clearly negative. This result is compatible with the mechanistic interpretation (see Scheme 1) that the rate-controlling first-order k_2 step is preceded by fast adduct formation. It is also important to point out that the rate-enhancing substituent effect of X = NO_2 in complexes Ni(XMesal-R)$_2$, as compared to X = Br (see Table 7), is due to an increase in K_{add}. The strongly electron-withdrawing nitro

(30) One might assume that reaction 6 proceeds only via the planar complex with second-order rate constant k_p, the size of which is not affected by R within the series of complexes Ni(*t*-BuMesal-R)$_2$. If so, the relationship $k_p = k_{H_2B}(1 + K_{p,t})$ should be valid. The numbers obtained for k_{H_2B} (Table 7) and $K_{p,t}$ (Table 6) do not confirm this assumption.

(31) If adduct formation precedes the rate-controlling k_2 step, the dependence $k_{obsd} = f([H_2B])$ should approach saturation-type behavior according to $k_{obsd} = k_2K_{add}[H_2B]/(1 + K_{add}[H_2B])$ at high $[H_2B]$. In the present system, limited solubility of the attacking ligands prevented studies at $[H_2B] > 0.05-0.1$ M. In the concentration range studied, the dependence $k_{obsd} = f([H_2B])$ was linear (see Figure 4).

group makes the nickel center a better Lewis acid and thus favors adduct formation.

Conclusions

Sterically demanding X substituents and R alkyl groups force bis(*N*-alkyl-X-salicylaldiminato)nickel(II) complexes Ni(Xsal-R)$_2$ = NiA_2 to leave the preferred planar trans-N_2O_2 coordination geometry and become more or less tetrahedrally distorted. In organic solution, there is a fast configurational change according to equilibrium a. The equilibrium constant $K_{p,t}$, the size of

$$NiA_2(\text{planar},S = 0) \overset{K_{p,t}}{\rightleftharpoons} NiA_2(\text{tetrahedral},S = 1) \quad \text{(a)}$$

which is determined by the bulkiness of X and R, is obtained from variable-temperature ^{1}H NMR measurements. In addition to equilibrium a, complexes NiA_2 tend to add bases such as pyridine according to equilibrium b. Ligand substitution in

$$NiA_2(\text{planar}) + 2py \overset{K_1}{\rightleftharpoons} NiA_2{\cdot}py + py \overset{K_2}{\rightleftharpoons} NiA_2{\cdot}2py \quad \text{(b)}$$

acetone according to reaction c with tetradentate ligands H_2B such as salen is monophasic and follows second-order kinetics.

$$NiA_2 + H_2B \xrightarrow{k_{H_2B}} NiB + 2HA \quad \text{(c)}$$

The effect of specific combinations of X and R on the size of β (= K_1K_2), $K_{p,t}$, and rate constant k_{H_2B} provides convincing evidence that ligand replacement according to equilibrium c is initiated by nucleophilic addition of H_2B to planar NiA_2 and formation of the adduct $NiA_2{\cdot}H_2B$. Loss of the first bidentate ligand HA is rate-determining.

Acknowledgment. Sponsorship of this work by the Deutsche Forschungsgemeinschaft, Verband der Chemischen Industrie e.V., and Otto-Röhm-Stiftung is gratefully acknowledged. Salicylaldehyde was kindly provided by Bayer AG.

Supporting Information Available: Tables of analytical data, crystallographic data, complete bond distances and bond angles, atomic positional parameters and anisotropic thermal parameters (14 pages). Ordering information is given on any current masthead page.

IC941454Y